Lattice design for an ILC damping ring with 3 km circumference

Andrzej Wolski

Lattice design for an ILC damping ring with 3 km circumference

Abstract

We describe a simple lattice that meets the specifications for the damping times and horizontal and longitudinal emittances for the International Linear Collider (ILC) damping rings. The circumference of a little over 3 km leads to a bunch spacing of around 3 ns, which will require advances in kicker technology for injection and extraction. We present the lattice design, and initial results of studies of the acceptance and collective effects. With the high bunch charge and close spacing, the ion and electron cloud effects are expected to be severe; however, the simple structure of the lattice allows for easy variation of the circumference and bunch spacing, which may make it useful for future investigations.

LBNL-56506

Lattice Design for an ILC Damping Ring with 3 km Circumference

A. Wolski
Lawrence Berkeley National Laboratory, Berkeley, CA 94720

October 18, 2004

Abstract

We describe a simple lattice that meets the specifications for the damping times and horizontal and longitudinal emittances for the International Linear Collider (ILC) damping rings. The circumference of a little over 3 km leads to a bunch spacing of around 3 ns, which will require advances in kicker technology for injection and extraction. We present the lattice design, and initial results of studies of the acceptance and collective effects. With the high bunch charge and close spacing, the ion and electron cloud effects are expected to be severe; however, the simple structure of the lattice allows for easy variation of the circumference and bunch spacing, which may make it useful for future investigations.

This work was supported by the Director, Office of Science, High Energy Physics, U.S. Department of Energy under Contract No. DE-AC03-76SF00098.

1 Introduction

The basic requirements of the ILC damping rings are that they accept a large beam from the particle sources, and produce a highly stable, low emittance beam for the downstream systems, at the machine repetition rate of 5 Hz. In the design of the lattice presented in this note, we use the specifications set out in the TESLA TDR [1]. The positron beam is expected to have a normalized emittance of 0.01 m (horizontal

and vertical), and the specified normalized emittances of the extracted beam are 8 μm horizontally and 0.02 μm vertically. Each bunch train consists of 2820 bunches with 2×10^{10} particles, and a nominal bunch separation of 337 ns in the main linac. This train must be compressed if the damping rings are to be of a reasonable size. The TESLA TDR specified damping rings of 17 km, with a bunch separation of 20 ns. Here, we explore the possibility of damping rings with a much lower circumference (around 3 km). We describe a simple lattice design together with the main parameters, and present the results of initial studies of the acceptance and some of the expected collective effects that may limit the performance of the damping rings. A ring with a 6 km circumference has already been proposed by Mishra et al [2]. Future work will compare the 17 km, 6 km and 3 km rings in more detail.

2 General Lattice Description

The main lattice parameters are given in Table 1, the synchrotron radiation integrals are given in Table 2, and the beam parameters are given in Table 3.

Table 1: General lattice parameters.

Energy	E	5.0 GeV
Circumference	C	3043.124 m
Revolution frequency	f_0	98.514 kHz
RF voltage	V_{RF}	13.12 MV
RF frequency	f_{RF}	650.00 MHz
Harmonic number	h	6598
Horizontal tune	ν_x	51.280
Vertical tune	ν_y	31.590
Synchrotron tune	ν_s	0.0269
Momentum compaction	α_p	2.88×10^{-4}
Natural bunch length	σ_z	6.00 mm
Natural energy spread	σ_δ	1.16×10^{-3}
RF acceptance	δ_{max}	1.98%
Energy loss per turn	U_0	5.34 MeV
Horizontal damping time	τ_x	19.0 ms
Vertical damping time	τ_y	19.0 ms
Longitudinal damping time	τ_ϵ	9.50 ms
Natural Emittance	ϵ_0	0.616 nm
Horizontal natural chromaticity	ξ_x	-128
Vertical natural chromaticity	ξ_y	-70.2

The lattice consists of 28 double-bend achromat (DBA) cells. In general, the natural emittance of a DBA lattice will be higher than that of a lattice at the same energy consisting of the same number of theoretical minimum emittance (TME) cells. Put another way, a larger number of DBA cells are needed to achieve a natural emittance below a given value, than if the lattice were constructed from TME cells. However, with the large circumference set by the length of the bunch train, the number of cells

Table 2: Synchrotron radiation integrals.

I_1	0.87632 m
I_2	0.60715 m^{-1}
I_3	0.044471 m^{-2}
I_4	2.0518×10^{-4} m^{-1}
I_5	1.0198×10^{-5} m^{-1}

Table 3: Beam parameters.

Particles per bunch	N_0	2.0×10^{10}
Number of bunches	n_b	2820
Bunch spacing	$\Delta\tau_b$	3.077 ns
Bunches per train	n_{train}	94
Bunches per gap		16
Number of bunch trains		30
Average current	$\langle I \rangle$	890 mA
Injected normalized emittance	$\gamma\epsilon_{inj}$	0.01 m
Equilibrium vertical emittance	$\gamma\epsilon_y$	0.02 μm

is not an important issue, and the DBA cell has the advantage of simplicity, since dispersion-free sections, necessary for the damping wiggler, occur naturally without the need for matching sections. It is also often the case that harmonic sextupoles, located outside the achromat, are helpful in improving the dynamic aperture. We did not find this to be the case in the present lattice; this is further discussed below.

The lattice functions in one periodic section of the lattice are shown in Figure 1. The lattice is tuned to give the optimum beta function in the dipole for minimum emittance with zero dispersion outside the achromat.

The tunes have been chosen with the following considerations:

- The vertical tune should be close to the half integer, to minimize sensitivity to quadrupole alignment errors. However, the tune should be sufficiently far from the half integer that the lattice is not overly sensitive to focusing errors.

- The working point should be away from major coupling resonances, to reduce sensitivity of the vertical emittance to sextupole misalignment and quadrupole rotation errors.

- The working point should be sufficiently far from major nonlinear resonances, to allow good dynamic aperture.

Ideally, in addition to the above considerations, the horizontal and vertical tunes should also be below the half-integer. Above the half-integer, the coupled-bunch mode most strongly driven by the resistive wall impedance is antidamped; below the half-integer, it is damped. However, the additional requirements on the bunch-by-bunch feedback system from operating slightly above the half-integer, compared to operating slightly below, are not that great. In the present case, it was found that a significantly better

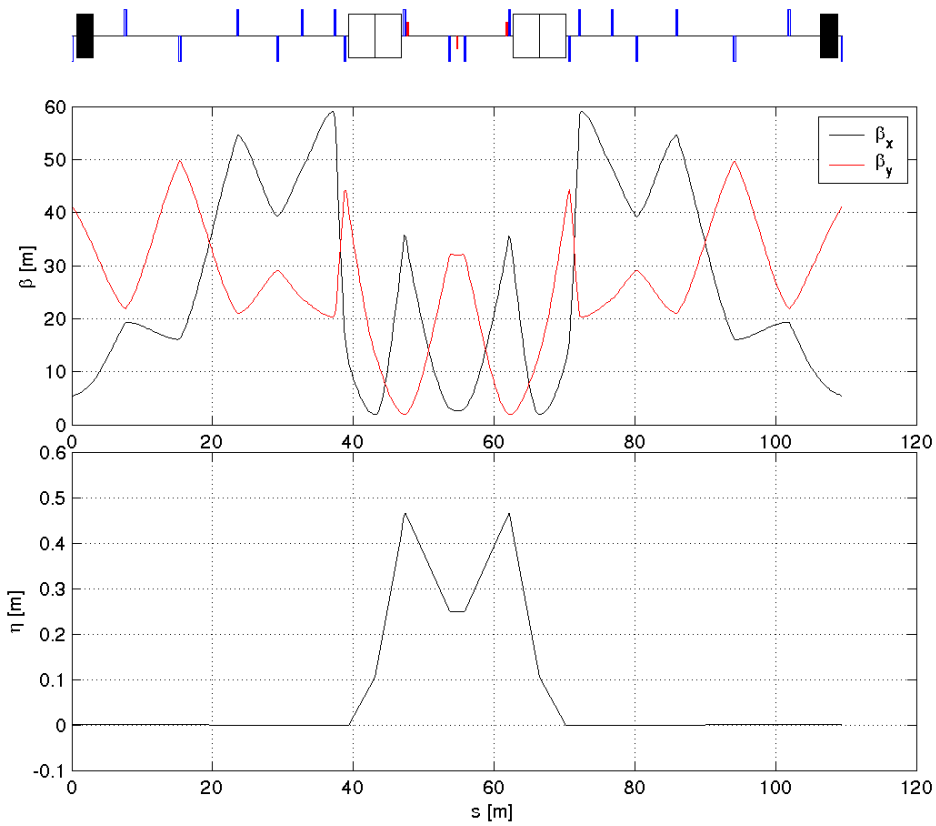

Figure 1: Beta functions and dispersion in one periodic section of the lattice.

dynamic aperture could be obtained with the vertical tune slightly above the half-integer.

2.1 Injection and Extraction Timing and RF System

The bunches are arranged in 30 trains of 94 bunches, with a gap of 16 "missing" bunches between bunch trains. The gaps are intended to prevent ion trapping. Extraction proceeds with the first bunch in each train; the gap after the last bunch train is one bunch shorter than the others, so that after the first bunch has been extracted from each train, extraction continues with the second bunch in each train with no delay in the arrival of bunches at the linac. Thus, the harmonic number must be a multiple of $30 \times (94 + 16) - 1 = 3299$. Choosing a harmonic number of 6598 with a circumference of 3043.124 m gives an RF frequency of 650 MHz, which is exactly half the main linac RF frequency of 1.3 GHz. The gap between bunches in the ring is 3.077 ns, and the spacing between bunches in the downstream systems is then a factor of $94 + 16 = 110$ times larger than this, or 338.47 ns.

The RF voltage of 13.12 MV has been chosen to give a bunch length of 6 mm. The RF acceptance at this voltage is a little under 2%, which should be sufficient to ensure good injection efficiency, but allows little margin for particles in the tails of the energy distribution. The required voltage may be provided by 26 RF cavities. There is sufficient room in the lattice to allow flexibility in the distribution of the cavities around the ring.

The locations of the injection and extraction components (kickers and septa) have not yet been specified.

2.2 Equilibrium and Extracted Emittance, and Alignment Sensitivity

The extracted emittance is given by:

$$\gamma\epsilon_{ext} = \mathrm{e}^{-2\frac{t}{\tau}}\gamma\epsilon_{inj} + \left(1 - \mathrm{e}^{-2\frac{t}{\tau}}\right)\gamma\epsilon_{equ} \tag{1}$$

where $\gamma\epsilon_{inj}$, $\gamma\epsilon_{ext}$, $\gamma\epsilon_{equ}$ are respectively the injected, extracted and equilibrium normalized emittances; t is the time after injection, and τ is the damping time. With an injected emittance of 0.01 m, an equilibrium vertical emittance of 0.02 μm, a damping time of 19.0 ms and a store time of 200 ms, the extracted vertical normalized emittance will be a negligible amount over 0.02 μm. This suggests that from point of view of the extracted emittance, the length (or field strength) of damping wiggler in the lattice could be reduced. It may be helpful to reduce the field strength from the present 1.4 T in order to increase the aperture; on the other hand, some 'excess' damping is desirable for better beam stability.

Again neglecting collective limitations, the extracted horizontal emittance will be essentially the equilibrium emittance, which at low coupling is close to the natural emittance. The natural emittance in the lattice described here is a little below the specified emittance of 8 μm for TESLA.

The minimum vertical emittance that can be achieved is determined by the vertical opening angle of the synchrotron radiation [3]:

$$\epsilon_y = \frac{13}{55}\frac{C_q}{J_y}\frac{\oint \frac{\beta_y}{|\rho|^3}\mathrm{d}s}{\oint \frac{1}{\rho^2}\mathrm{d}s} \tag{2}$$

For the present lattice, the minimum vertical emittance (not normalized) is 0.24 pm, or 12% of the specified operating vertical emittance.

An equilibrium vertical normalized emittance of 0.02 μm is a challenging goal that will require precise magnet alignment and correction of the vertical dispersion and betatron coupling. The sensitivity of the vertical orbit, dispersion and coupling to magnet motion are relevant quantities, which depend on the magnet strengths and lattice functions. To quantify the sensitivities, it is convenient first to define the following quantities:

$$\Sigma_{1\mathrm{O}} = \sum_{\text{quadrupoles}} \beta_y (k_1 L)^2 \tag{3}$$

$$\Sigma_{1\mathrm{D}} = \sum_{\text{quadrupoles}} \beta_y \eta_x^2 (k_1 L)^2 \tag{4}$$

$$\Sigma_{1\mathrm{C}} = \sum_{\text{quadrupoles}} \beta_x \beta_y (k_1 L)^2 \tag{5}$$

$$\Sigma_{2\mathrm{D}} = \sum_{\text{sextupoles}} \beta_y \eta_x^2 (k_2 L)^2 \tag{6}$$

$$\Sigma_{2\mathrm{C}} = \sum_{\text{sextupoles}} \beta_x \beta_y (k_2 L)^2 \tag{7}$$

The numeric subscript on the Σ_{**} indicates whether the summation is performed over the quadrupoles or the sextupoles, and the alphabetic subscript identifies the quantity as relevant for the orbit, dispersion, or betatron coupling. The $k_1 L$ are the integrated normalized quadrupole strengths, and the $k_2 L$ are the integrated normalized sextupole strengths.

In terms of the above quantities, we can write the following approximate relationships:

$$\frac{\langle y^2 \rangle}{\langle \sigma_y^2 \rangle} \simeq \frac{\langle \Delta Y_q^2 \rangle}{8\epsilon_y \sin^2 \pi\nu_y} \Sigma_{1\mathrm{O}} \tag{8}$$

$$\frac{\epsilon_y}{\langle \Delta\Theta_q^2 \rangle} \simeq \frac{J_x}{J_y} \frac{1 - \cos 2\pi\nu_x \cos 2\pi\nu_y}{\left(\cos 2\pi\nu_x - \cos 2\pi\nu_y\right)^2} \epsilon_x \Sigma_{1\mathrm{C}} + J_\epsilon \frac{\sigma_\delta^2}{\sin^2 \pi\nu_y} \Sigma_{1\mathrm{D}} \tag{9}$$

$$\frac{\epsilon_y}{\langle \Delta Y_s^2 \rangle} \simeq \frac{J_x}{J_y} \frac{1 - \cos 2\pi\nu_x \cos 2\pi\nu_y}{4\left(\cos 2\pi\nu_x - \cos 2\pi\nu_y\right)^2} \epsilon_x \Sigma_{2\mathrm{C}} + J_\epsilon \frac{\sigma_\delta^2}{4\sin^2 \pi\nu_y} \Sigma_{2\mathrm{D}} \tag{10}$$

Here, $\langle y^2 \rangle$ is the mean square vertical orbit distortion; $\langle \Delta Y_q^2 \rangle$ is the mean square vertical quadrupole misalignment; $\langle \Delta Y_s^2 \rangle$ is the mean square vertical sextupole misalignment; $\langle \Delta\Theta_q^2 \rangle$ is the mean square quadrupole rotation about the beam axis; J_x, J_y and J_ϵ are the damping partition numbers; ν_x and ν_y are the betatron tunes, and σ_δ is the rms natural energy spread. These expressions assume that the misalignments are random and uncorrelated, that the betatron coupling is dominated by the lowest-order difference resonance, and that the dispersion in the dipoles and wigglers is not correlated. These assumptions are not necessarily valid for the damping rings. In particular, when calculating the contribution of the vertical dispersion to the emittance, it can be important to consider the dispersion in the wiggler separately from the rest of the lattice. This is because the radiation from the wiggler typically dominates over

the radiation from the dipoles. This emphasizes the need to study the emittance tuning by detailed simulations; however, bearing these issues in mind, we can proceed to estimate the sensitivities of the different lattices.

We define the following three measures of the lattice sensitivity:

Quadrupole jitter sensitivity is the rms quadrupole misalignment that will generate an orbit distortion equal to the beam size for a specified emittance. This is found from (8).

Quadrupole rotation sensitivity is the rms quadrupole rotation that will generate a specified vertical emittance. This is found from (9).

Sextupole alignment sensitivity is the rms sextupole vertical misalignment that will generate a specified vertical emittance. This is found from (10).

The values of these sensitivities for the present lattice are given in Table 4. The values are typical for a large storage ring operating with an emittance ratio of around 0.3%.

Table 4: Lattice sensitivities.

Quadrupole Jitter	226 nm
Quadrupole Rotation	349 μrad
Sextupole Alignment	67 μm

2.3 Dipoles, Quadrupoles, Sextupoles and Octupoles

One of the difficulties with large, low-emittance lattice designs is that the low dispersion leads to a small momentum compaction, which in turn makes the beam sensitive to a variety of collective effects. This can be compensated by using long, low-field dipoles. In the present design, the dipoles are a little under 7.5 m long, with a field of 0.25 T.

The parameters of the dipoles and higher multipoles are shown in Table 5. We have assumed a full aperture of 60 mm for all magnets, which will allow a vacuum chamber inside radius of 25 mm. this gives a reasonable pole-tip field for all magnets. There is sufficient room in the lattice to allow flexibility in the lengths of the magnets, to increase the aperture while reducing the pole-tip field if necessary. Note that at present, all magnets of a given type have the same length and aperture.

Table 5: Parameters of dipoles and strongest multipoles.

Type	Length [m]	Field or Gradient	Full Aperture [m]	Pole-tip field [T]
Dipoles	7.485	0.250 T	0.06	0.250
Quadrupoles	0.30	20.7 T/m	0.06	0.621
Sextupoles	0.20	170 T/m^2	0.06	0.0765
Octupoles	0.20	3580 T/m^3	0.06	0.0161

2.4 Damping Wiggler

The wiggler parameters are given in Table 6. Note that the ends of the wiggler are designed so that the orbit is centered on the wiggler axis; the length of each wiggler section is therefore not exactly the period length multiplied by the given number of periods per section. It is desirable to have as large a physical aperture as possible in the wiggler; this is constrained by the field strength requirements, and we have chosen fairly conservative values for the peak field and the period. A hard-edged dipole model is used at present in the lattice. A more realistic model, including focusing adjustments and nonlinear terms, will need some magnet design work.

Table 6: Wiggler parameters.

Period	λ_w	400 mm
Peak field	$\hat{B}_w$	1.40 T
Periods per wiggler		6.5
Total number of wigglers		56
Total length of wiggler		138 m

2.5 Vacuum System

Some parameters of the vacuum system are needed for estimates of certain collective effects. We assume the parameters given in Table 7. The circular cross-section is an approximation for purposes of estimates of resistive-wall effects. The challenging specification on the residual gas pressure (0.1 ntorr) is driven by the ion effects, and will probably require an antechamber.

Table 7: Vacuum system parameters.

Vacuum chamber material		aluminum
Beam pipe conductivity	σ_c	$3.8\times10^7\Omega^{-1}\mathrm{m}^{-1}$
Vacuum chamber cross-section		circular
Beam-pipe radius (except wiggler)		25 mm
Beam-pipe radius (in wiggler)		15 mm
Mean beam-pipe radius	$\langle b \rangle$	24.2 mm
Residual gas pressure	p_0	0.1 ntorr

3 Nonlinear Dynamics and Dynamic Aperture

3.1 Tune Shifts with Energy and Betatron Amplitude

The sextupoles are tuned to give zero linear chromaticity. Their locations have been chosen to minimize the strengths required for this purpose, i.e. the sextupole locations have large dispersion and good separation of the horizontal and vertical beta functions. The remaining tune-shifts with energy are dominated by the second-order terms; this is shown in Figure 2.

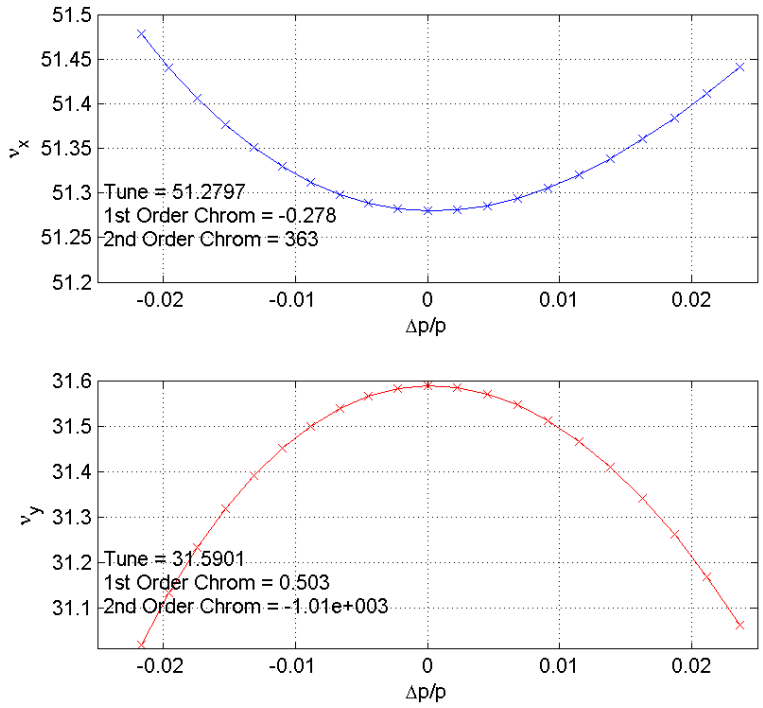

Figure 2: Tune shifts with energy.

The sextupoles cause large variations in the tunes with betatron amplitude. Conventionally, such nonlinear effects are compensated in a DBA lattice by the use of harmonic or auxiliary sextupoles outside the achromat. In the present case, we found that auxiliary sextupoles had little benefit for the dynamic aperture. Instead, we used octupoles to control the tune shifts with amplitude. The horizontal and vertical tunes for different values of the betatron actions are shown in Figure 3 (octupoles off) and Figure 4 (octupoles on).

3.2 Transverse Phase Space

An indication of the strength of the nonlinear dynamics can be found from plotting the phase-space portraits in the horizontal and vertical planes. The nonlinear elements in the lattice distort the phase-space invariants from the ellipses that are expected in a linear system. The phase-space portraits for the lattice with the octupoles off are shown in Figure 5, and with the octupoles on in Figure 6. In each plot, the beta functions at the observation point are $\beta_x = 5.45$ m, $\beta_y = 41.1$ m. Particles are initially spaced at intervals corresponding to half the rms injected beam size (assuming an injected emittance of 0.01 m normalized), and tracked for 500 turns.

The octupoles appear to have a detrimental effect on the stability of orbits at large horizontal betatron amplitude; however, we found this to be limited to the case where the vertical betatron amplitude was small. For large horizontal and vertical betatron amplitudes, the octupoles do improve the stability. This is consistent with the large cross-plane tune shifts seen in Figure 3.

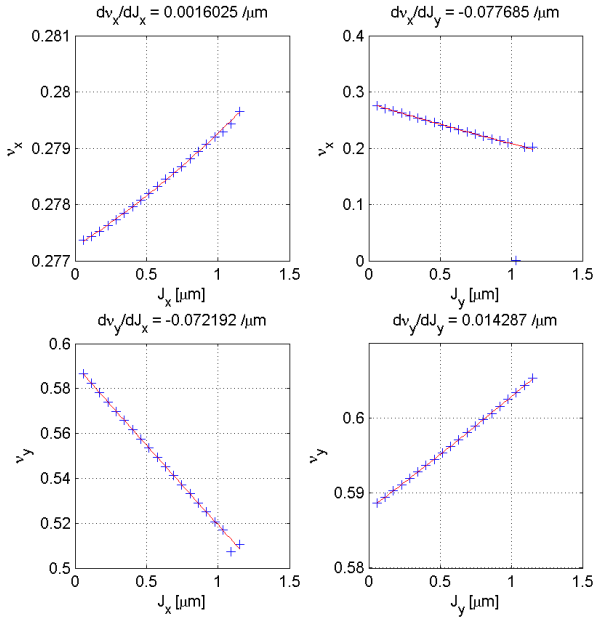

Figure 3: Tune shifts with betatron amplitude, with octupoles off.

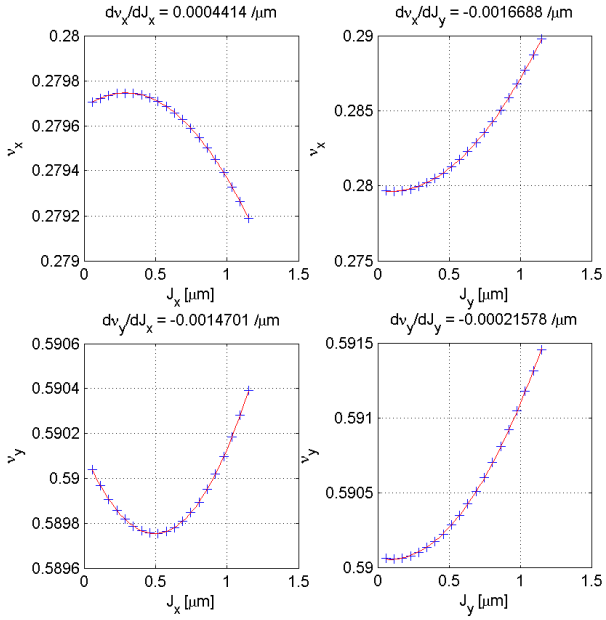

Figure 4: Tune shifts with betatron amplitude, with octupoles on.

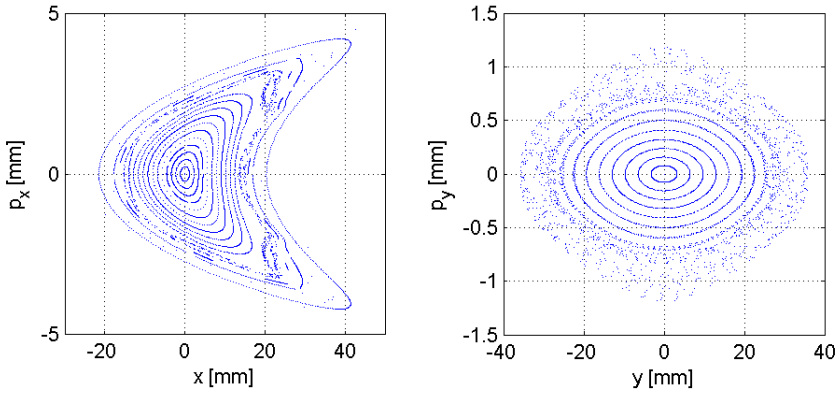

Figure 5: Phase-space portraits, with octupoles off.

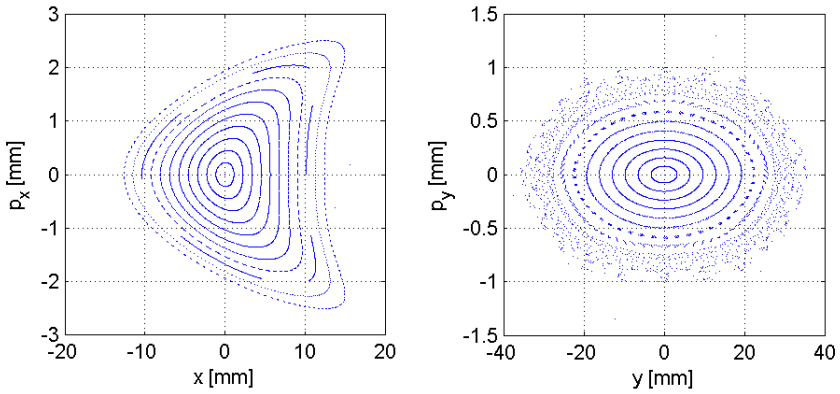

Figure 6: Phase-space portraits, with octupoles on.

3.3 Dynamic Aperture: Frequency Map Analysis

A more detailed picture of the nonlinear dynamics can be obtained using Frequency Map Analysis. This technique has been used successfully to improve the acceptance of the LBNL Advanced Light Source [4], [5], [6]. Briefly, we track particles at different betatron amplitudes, and analyze the tracking data using an interpolated Fourier-Hanning technique to determine the tunes with high precision. Corresponding points are plotted in co-ordinate space and tune space. A "diffusion rate" in tune space is determined by tracking for $2N$ turns, and comparing the difference in tune between the first N turns and the last N turns. The diffusion rate is indicated by a color scale on both the co-ordinate space and tune space plots. Strong resonances are often characterized by rapid diffusion.

The dynamic aperture in co-ordinate space and the corresponding frequency map are shown in Figure 7. Particles were tracked for 256 turns; all results in this section are for the lattice with the octupoles turned on. The diffusion rate is given on a logarithmic scale: a value of -6, for example, means that change in the horizontal and vertical tunes between the first 128 and the last 128 turns, is 10^{-6} (note that the changes in the tune are added in quadrature). As with the phase-space portraits, the beta functions at the observation point are $\beta_x = 5.45$ m, $\beta_y = 41.1$ m. Assuming an injected normalized emittance of 0.01 m, the corresponding rms beam sizes are $\sigma_x = 2.36$ mm and $\sigma_y = 6.48$ mm. The acceptance is of the order of four times the beam size horizontally, and five times the beam size vertically. Magnet errors, including systematic and random multipole components in the wiggler and other magnets, and tuning errors, can be expected to reduce the dynamic aperture significantly, and the present acceptance of the lattice is probably insufficient to ensure the necessary injection efficiency.

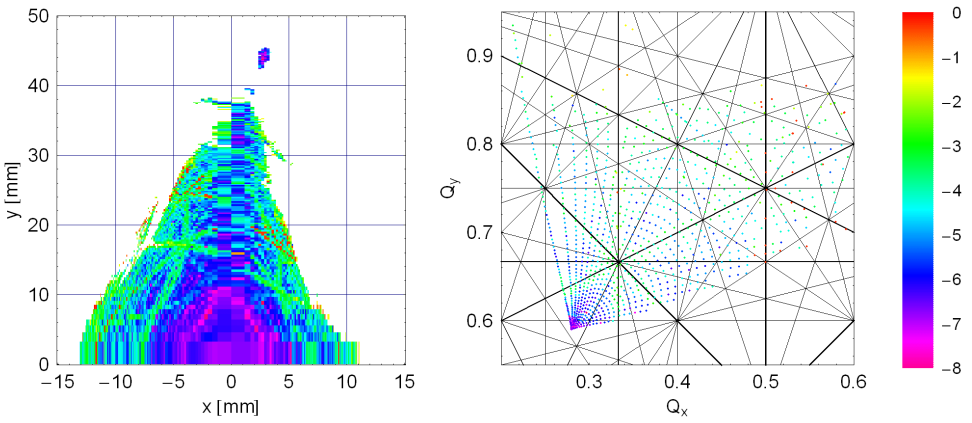

Figure 7: Dynamic aperture in co-ordinate space and frequency map. The nominal injected beam sizes are $\sigma_x = 2.36$ mm and $\sigma_y = 6.48$ mm. The nominal fractional tunes are (0.28,0.59). Resonance lines up to fifth order are shown.

Figure 8 shows the dynamic aperture and corresponding frequency map in $\delta - x$ space. The dynamic energy acceptance is close to $\pm 3\%$, and larger than the RF acceptance.

Finally, we emphasize that the results presented here are preliminary. Further

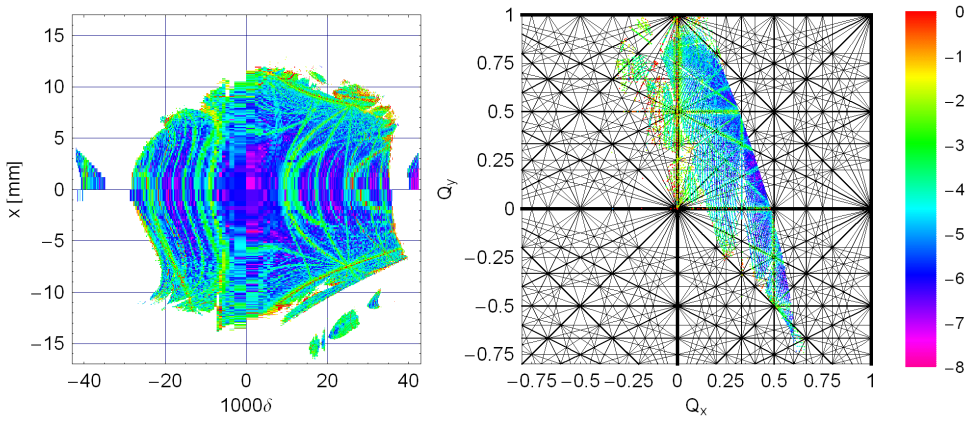

Figure 8: Dynamic aperture in $\delta - x$ space and frequency map. The nominal injected beam sizes are $\sigma_x = 2.36$ mm and $\sigma_y = 6.48$ mm. The nominal fractional tunes are (0.28,0.59). Resonance lines up to fifth order are shown.

optimization of the nonlinear dynamics is likely to be possible, and would likely involve changes to sextupoles and octupoles. Also, the effects of errors, which are expected to reduce the dynamic aperture significantly, need careful study.

4 Collective Effects

In this section, we present the results of initial estimates of the severity of a variety of collective effects expected to be important. Many of the phenomena we consider need a more careful analysis than we have carried out at the present time; the results here should be interpreted only as general indications of the severity of the relevant effects.

4.1 Microwave and CSR Instability

The Keill-Schnell-Boussard criterion gives an impedance threshold for the longitudinal microwave instability that may be written:

$$\frac{Z_{//}}{n} = Z_0 \sqrt{\frac{\pi}{2}} \frac{\gamma \alpha_p \sigma_\delta^2 \sigma_z}{N_0 r_e} \tag{11}$$

where Z_0 is the free-space impedance, γ the relativistic factor, and r_e the classical electron radius. There is also a transverse coasting-beam instability associated with the transverse impedance. Again applying the Keill-Schnell-Boussard criterion, the threshold for this instability may be written:

$$Z_\perp = Z_0 \frac{\gamma \alpha_p \sigma_\delta \nu_y}{N_0 r_e} \frac{\omega_0 \sigma_z}{c} \tag{12}$$

Although the relationship is strictly true only for the resistive wall impedance, the transverse broad-band impedance is often assumed to be related to the longitudinal broad-band impedance through:

$$Z_\perp = \frac{2c}{\omega_0 \langle b \rangle^2} \frac{Z_{//}}{n} \tag{13}$$

where $\langle b \rangle$ is the mean vacuum chamber radius.

Coherent synchrotron radiation is also able to drive beam instabilities; the threshold is given as a bunch charge above which, the CSR instability starts to have an effect [7]:

$$N_{0,th} = 3.6 \frac{C}{4\pi\langle b \rangle} \frac{\gamma \alpha_p \sigma_\delta^2 \sigma_z}{r_e} \tag{14}$$

Using appropriate values for the parameters, we can evaluate all the above thresholds. The results are given in Table 8.

Table 8: Microwave and CSR instability thresholds.

Longitudinal broad-band impedance threshold	$\frac{Z_{//}}{n}$	191 mΩ
Transverse broad-band impedance threshold	$Z_\perp$	4.3 MΩ/m
Longitudinal equivalent impedance threshold	$\frac{\omega_0 \langle b \rangle^2}{2c} Z_\perp$	2630 mΩ
CSR instability charge threshold	$N_{0,th}$	2.9×10^{11}

4.2 Space-Charge Tune Shift

Space-charge forces lead to a significant vertical tune shift, because of the large circumference and small vertical beam size. The incoherent tune shift is given by:

$$\Delta\nu_y = \frac{N_0 r_e}{\sqrt{2\pi}^3 \gamma^3 \sigma_z} \int_0^C \frac{\beta_y}{\sigma_y \left(\sigma_x + \sigma_y\right)} \mathrm{d}s \tag{15}$$

Evaluating the integral gives an incoherent space-charge tune shift of 0.052 which, while significant, should not in itself prevent operation of the damping rings with their specificied parameters.

4.3 Resistive-Wall Instability

The resistive-wall impedance of the vacuum chamber will drive a transverse coupled-bunch instability. The impedance is given by:

$$Z_\perp(\omega) = \left(1 - \mathrm{sgn}\left(\omega\right) \mathrm{i}\right) Z_0 \frac{C}{2\pi\langle b \rangle^3} \delta_{\mathrm{skin}}(\omega) \tag{16}$$

where the skin depth is:

$$\delta_{\mathrm{skin}} = \sqrt{\frac{2}{\sigma_c \mu_c \omega}} \tag{17}$$

σ_c and μ_c are the conductivity and magnetic permeability of the vacuum chamber. Assuming a uniform fill of n_b bunches with average current $\langle I \rangle$, the growth rate of a transverse mode with mode number m is given by:

$$\frac{1}{\tau_m} = -\frac{c\langle I \rangle}{4\pi\nu_y E/e} \mathrm{Re} \sum_{p=-\infty}^{\infty} Z_\perp\left(\left(\nu_y + n_b p + m\right)\omega_0\right) \tag{18}$$

With the nominal operating conditions, the ring is not uniformly filled, but there are gaps between bunch trains. We can still estimate the growth rates by assuming a

uniform fill, but either using the same average current as in the case where there are gaps between bunch trains, or using the same bunch charge. Using the same average current will likely underestimate the growth rates; using the same bunch charge will likely overestimate the growth rates. In the present case, the gaps account for roughly 16% of the circumference, so the difference between the two cases is not large.

Figure 9 shows the growth rates of the unstable modes in the vertical plane, assuming a uniform fill. The red (upper) points show the growth rates with the same charge per bunch as the nominal case; the black (lower) points show the growth rates with the same average current as the nominal case. The blue broken line shows the vertical damping time.

Table 9 gives the growth time of the instability, and the range of unstable modes with growth rates faster than the radiation damping rate. A bunch-by-bunch feedback system will be needed to suppress the instability; a potential concern is the jitter induced on the beam by the feedback system.

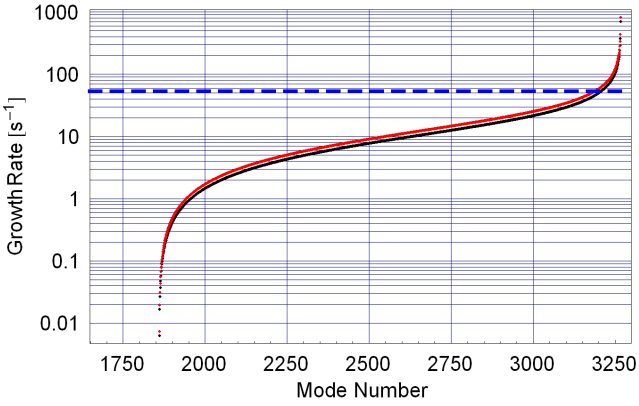

Figure 9: Growth rates of unstable resistive-wall modes.

Table 9: Resistive wall instability growth times, assuming uniform fill at nominal bunch charge.

Shortest growth time	1.22 ms
Shortest growth time	120 turns
Lowest unstable mode number	3187
Highest unstable mode number	3267

We note that higher-order modes in the RF cavities can also drive coupled-bunch instabilities. The RF cavity design is not known at the present time, so we have not investigated these growth rates.

4.4 Ion Effects

First, we consider ion trapping. Without gaps in the fill, ions with a relative molecular mass greater than $A_{x(y)}$ will be trapped horizontally (vertically), where

$$A_{x(y)} = \frac{N_0 r_p c \Delta\tau_b}{2\sigma_{x(y)}\left(\sigma_x + \sigma_y\right)} \tag{19}$$

At the equilibrium beam size, all ions will be trapped horizontally, and ions with a relative molecular mass greater than 11 will be trapped vertically. Other ions will be trapped vertically as the beam damps from its injected size.

It is hoped that the gaps in the fill will be sufficient to clear ions accumulated during the passage of a bunch train. However, we must then consider the fast-ion instability arising from the ions accumulated during one bunch train [8]. The line density of ions at the end of a bunch train is given by:

$$\lambda_{\mathrm{ion}} = N_0 n_{\mathrm{train}} \frac{p_0}{kT} \sigma_{\mathrm{ion}} \tag{20}$$

where σ_{ion} is the ionization cross-section, assumed to be 2 Mb. The presence of the ions causes coherent and incoherent tune shifts, with the incoherent tune shift twice as large as the coherent. Because of the small vertical beam size, the effects are much stronger in the vertical plane. The incoherent vertical tune shift is given by:

$$\Delta\nu_y = \frac{1}{2\pi}\int_0^C K_y \beta_y \mathrm{d}s \tag{21}$$

where the ion focusing is given by:

$$K_y = \frac{\lambda_{\mathrm{ion}} r_e}{\gamma\sigma_y\left(\sigma_x + \sigma_y\right)} \tag{22}$$

As well as the tune shifts, there is a growth in betatron oscillations of bunches towards the rear of the bunch train, driven by oscillations of the ions in the potential of the beam. The ion oscillation frequency is ω_{ion}, given by:

$$\frac{\omega_{\mathrm{ion}}^2}{c^2} = \frac{\bar{\lambda}_e r_p}{A\sigma_y\left(\sigma_x + \sigma_y\right)} \tag{23}$$

where $\bar{\lambda}_e = N_0/c\Delta\tau_b$ is the mean line density of electrons in the beam, A is the relative molecular mass of the residual gas ions in the chamber, and r_p is the classical radius of the proton. The growth rate of betatron oscillations of bunches towards the rear of the bunch train is given by:

$$\frac{1}{\tau} = \frac{f_0}{4\sqrt{2}\sigma_\omega}\int_0^C \omega_{\mathrm{ion}} K_y \beta_y \mathrm{d}s \tag{24}$$

where f_0 is the revolution frequency, and σ_ω is the standard deviation of the ion oscillation frequency around the ring, resulting from the variation in beam size.

Table 10 gives the parameters of the fast-ion instability, found by applying the above expressions to the present lattice design. We assume that the dominant gas species in the chamber is CO.

Table 10: Parameters of the fast-ion instability.

Residual vacuum pressure	p_0	0.1 ntorr
Molecular mass of residual gas (species)	A	28 (CO)
Ion density at end of bunch train	$\lambda_{\rm ion}$	$1.2 \times 10^3 {\rm m}^{-1}$
Mean ion frequency	$\omega_{\rm ion}/c$	1.08 ${\rm m}^{-1}$
Standard deviation ion frequency	σ_ω/c	0.21 ${\rm m}^{-1}$
Incoherent vertical tune shift	$\Delta\nu_y$	0.0046
Exponential growth time	τ	360 μs

At 0.1 ntorr residual gas pressure, the incoherent tune shift is small enough not to limit operational performance. The exponential growth time is fast, but it should be possible to suppress the instability using a bunch-by-bunch feedback system; as with the resistive wall instability, the concern is the jitter that such a feedback system could induce on the beam. Emittance growth will be associated with the coherent bunch oscillations driven by the accumulated ions. The simple estimates used here indicate that ion effects are likely to be an issue in the damping ring. Further studies, including simulations and experimental work, will be needed to predict the impact on machine performance with more confidence.

4.5 Electron Cloud Effects

Electrons accumulating in the positron damping ring may have a multitude of dynamical effects on the beam, including single bunch and coupled bunch instabilities. Here, we consider only the single bunch effects. We treat the electron cloud as a broadband transverse impedance, with resonant frequency characteristic of the oscillation frequency of the electrons in the potential of a single positron bunch. This frequency $\omega_{\rm ecloud}$ is given by:

$$\frac{\omega_{\rm cloud}^2}{c^2} = \frac{N_0 r_e}{\sqrt{2\pi}\sigma_z\sigma_y\left(\sigma_x+\sigma_y\right)} \tag{25}$$

In the present case, the oscillation frequency is large compared to the bunch length (see Table 11), so it is appropriate to use a coasting-beam model for the instability. Following Ohmi and Zimmermann [9], we estimate the transverse impedance from the electron cloud as:

$$Z_\perp = Z_0 C \frac{\hat{\rho}_{\rm cloud}}{2\lambda_{\rm beam}} \tag{26}$$

where $\hat{\rho}_{\rm cloud}$ is the peak cloud density in the beam, and $\lambda_{\rm beam} = N_0/\sqrt{2\pi}\sigma_z$ is the peak line density of charge in the beam. Using the Keill-Schnell-Boussard criterion, the instability threshold is:

$$Z_{\perp,th} = Z_0 \frac{\gamma\alpha_p\sigma_\delta\nu_y}{N_0 r_e}\frac{\omega_{\rm cloud}\sigma_z}{c} \tag{27}$$

Combining equations (26) and (27) gives the electron cloud density threshold at which instability occurs:

$$\hat{\rho}_{\rm cloud} = \sqrt{\frac{2}{\pi}}\frac{\gamma\alpha_p\sigma_\delta\nu_y}{r_e}\frac{\omega_{\rm cloud}}{cC} \tag{28}$$

This may be compared with the mean density of electrons in the chamber expected from the neutralization condition:

$$\rho_{\rm neut} = \frac{N_0}{\pi \langle b \rangle^2 c \Delta \tau_b} \tag{29}$$

Values are given in Table 11. The instability threshold is nearly a factor of two higher than neutralization density. However, the neutralization density is an average density that does not include the enhancement that can occur during a bunch passage. Simulations suggest that the density of the cloud in the bunch can be increased by an order of magnitude during a bunch passage. In this case, an instability will occur. It appears necessary to reduce the density of the cloud in the chamber at least by an order of magnitude below the neutralization level to prevent an instability.

Table 11: Parameters of the electron-cloud instability.

Cloud oscillation frequency	$\omega_{\rm cloud}/c$	1920 $\rm m^{-1}$
Cloud oscillations per bunch	$\omega_{\rm cloud}\sigma_z/c$	11.5
Instability impedance threshold	$Z_\perp$	7.97 MΩ/m
Instability cloud density threshold	$\hat{\rho}_{\rm cloud}$	1.85×10^{13} $\rm m^{-3}$
Neutralization density	$\rho_{\rm neut}$	1.18×10^{13} $\rm m^{-3}$

4.6 Touschek Lifetime

The beam store time is around 200 ms, which is much less than the Touschek lifetime. However, a reasonable Touschek lifetime is desirable for commissioning and tuning. For flat beams that are non-relativistic in the beam rest frame, and assuming that the energy aperture is given by the RF acceptance δ_{max}, the Touschek lifetime τ is given by [10]:

$$\frac{1}{\tau} = \frac{r_e^2 c N_0}{8\pi\gamma^2 \delta_{max}^3 \sigma_z} \frac{1}{C} \int_0^C \frac{D(\epsilon)}{\sigma_x \sigma_y} {\rm d}s \tag{30}$$

where the function $D(\epsilon)$ is defined by:

$$D(\epsilon) = \sqrt{\epsilon}\left[-\frac{3}{2}{\rm e}^{-\epsilon} + \frac{\epsilon}{2}\int_\epsilon^\infty \frac{\ln u}{u}{\rm e}^{-u}{\rm d}u + \frac{1}{2}\left(3\epsilon - \epsilon\ln\epsilon + 2\right)\int_\epsilon^\infty \frac{{\rm e}^{-u}}{u}{\rm d}u\right] \tag{31}$$

and the argument ϵ is given by:

$$\epsilon = \left(\frac{\delta_{max}\beta_x}{\gamma\sigma_x}\right)^2 \tag{32}$$

With an energy acceptance of 1.98%, the Touschek lifetime is 155 minutes. This is a reasonable beam lifetime for commissioning and tuning purposes; however, we note that the lifetime drops rapidly with decreasing energy acceptance, so dynamic limits on the energy acceptance could have a significant impact.

4.7 Intrabeam Scattering

As well as the large-angle scattering leading to particle loss (Touschek effect), particles within a bunch undergo small-angle scattering. The resulting increases in the beam emittances are described by the theory of intrabeam scattering (IBS). To calculate the emittance growth in the present lattice, we use the approximation of Bane [11] to the theory of Bjorken and Mtingwa [12]. In Bane's approximation, the growth rate of the energy spread resulting from intrabeam scattering is given by:

$$\frac{1}{T_p} = \frac{r_e^2 c N_0}{16\gamma^3 \sqrt[4]{\beta_x \epsilon_x^3 \beta_y \epsilon_y^3}\sigma_z \sigma_\delta^3} \ln\left(\frac{\sqrt{\beta_y \epsilon_y}\gamma^2 \epsilon_x}{r_e \beta_x}\right) g\left(\sqrt{\frac{\beta_x \epsilon_y}{\beta_y \epsilon_x}}\right) \sigma_H \tag{33}$$

where the auxiliary functions are defined:

$$\sigma_H = \left(\frac{1}{\sigma_\delta^2} + \frac{\mathcal{H}_x}{\epsilon_x} + \frac{\mathcal{H}_y}{\epsilon_y}\right)^{-\frac{1}{2}} \tag{34}$$

and:

$$g(\alpha) = \alpha^{0.021 - 0.044 \ln \alpha} \quad \alpha \leq 1 \tag{35}$$

$$g(\alpha) = g(1/\alpha) \quad \alpha > 1 \tag{36}$$

$\mathcal{H}_x$ is the dispersion H-function:

$$\mathcal{H}_x = \gamma_x \eta_x^2 + 2\alpha \eta_x \eta_x' + \beta_x \eta_x'^2 \tag{37}$$

In the limit in which the vertical emittance is generated entirely by vertical dispersion (i.e. with no betatron coupling) the horizontal and vertical growth rates are given by:

$$\frac{1}{T_x} = \sigma_\delta^2 \frac{\mathcal{H}_x}{\epsilon_x} \frac{1}{T_p} \tag{38}$$

$$\frac{1}{T_y} = \sigma_\delta^2 \frac{\mathcal{H}_y}{\epsilon_y} \frac{1}{T_p} \tag{39}$$

The vertical dispersion arises from vertical steering errors. For our calculations, we use an average value determined from the usual expression for the equilibrium emittance in the presence of radiation damping and quantum excitation:

$$\epsilon_y = C_q \gamma^2 \langle \mathcal{H}_y \rangle \frac{I_3}{I_2} \tag{40}$$

For an equilibrium vertical emittance of 2 pm, this gives $\langle \mathcal{H}_y \rangle = 0.744$ μm. Assuming uncorrelated errors, we can write an approximate relationship between the dispersion and the dispersion H-function:

$$\langle \mathcal{H}_y \rangle \approx \frac{\langle \eta_y^2 \rangle}{\langle \beta_y \rangle} \tag{41}$$

With $\langle \beta_y \rangle = 25.8$ m, this gives an rms vertical dispersion of 4.3 mm. As mentioned above, our treatment assumes that the vertical emittance is generated entirely by vertical dispersion.

The emittances $\epsilon_{x,N}$ and $\epsilon_{y,N}$ with a bunch charge N in the presence of intrabeam scattering are found from: the zero-current emittances ϵ_x and ϵ_y; the IBS growth times T_x and T_y; the synchrotron radiation damping times τ_x and τ_y. In the horizontal plane:

$$\epsilon_{x,N} = \frac{T_x}{T_x - \tau_x}\epsilon_x \tag{42}$$

A similar equation holds for the vertical plane. For the energy spread, we have:

$$\sigma_{\delta,N} = \frac{T_p}{T_p - \tau_p}\sigma_\delta \tag{43}$$

where τ_p is the longitudinal radiation damping time, and $\sigma_{\delta,N}$ is the energy spread with a bunch charge N. A similar equation holds for the bunch length. Since the growth rates depend on the beam emittances, the equilibrium emittances for a given bunch charge need to be found by iteration. Also note that the growth rates need to be averaged around the ring. Performing the calculations for the present lattice gives the results shown in Table 12. Note that the proportional growth in the bunch length is equal to the proportional growth in the energy spread.

Table 12: Intrabeam scattering growth rates and emittance growths.

Bunch charge	N	2×10^{10}
Horizontal growth time	T_x	0.109 s
Vertical growth time	T_y	1.88 s
Longitudinal growth time	T_p	0.483 s
Horizontal emittance growth	$\epsilon_{x,N}/\epsilon_x - 1$	21%
Vertical emittance growth	$\epsilon_{y,N}/\epsilon_y - 1$	1.9%
Energy spread growth	$\sigma_{\delta,N}/\sigma_\delta - 1$	1.9%

The growth in the horizontal emittance at the nominal bunch charge is not negligible, but is still within the specified operating value of 8μm. The growths in the vertical and longitudinal planes are much smaller. In the case that the vertical emittance is generated entirely by betatron coupling (as opposed to vertical dispersion, as we have assumed here), the proportional growth in the vertical emittance will be equal to the proportional growth in the horizontal emittance. In practice, therefore, we expect the proportional growth in the vertical emittance to lie somewhere between 2% and 21%. An emittance growth at the upper end of the range could have some impact on machine performance.

5 Summary and Conclusions

The lattice design we have discussed meets the principal specifications for damping time and extracted emittance. With a circumference of a little over 3 km, the bunch spacing is around 3 ns, which sets a challenging specification for the injection and extraction kickers. Initial analysis of the single-particle and multi-particle beam dynamics suggests that the required performance could be achieved in this lattice, but there are a number of issues which need to be addressed in more detail. Specifically:

- The acceptance of the lattice will need to be improved to ensure close to 100% injection efficiency. Presently, the dynamic aperture is four times the injected rms beam size horizontally, and five times the injected rms beam size vertically. The energy acceptance is close to 3%. When errors are included, the acceptance can be expected to reduce significantly.

- The incoherent space-charge tune shift is expected to be around 0.05, which should be tolerable. However, detailed tracking studies are needed to determine if the tune shift leads to emittance growth or particle loss.

- The Keill-Schnell-Boussard criterion indicates that the longitudinal microwave instability will occur if the longitudinal broad-band impedance is above 190 mΩ. This sets a demanding specification on the design and construction of the vacuum chamber. However, a more detailed analysis, using realistic functions for the wake fields of individual components, will be required to specify the impedance limit with more confidence. The threshold for the transverse instability is much higher than for the longitudinal instability.

- A bunch-by-bunch feedback system will be needed to suppress the coupled-bunch instability driven by the resistive-wall impedance. The expected growth times are around 120 turns. The feedback system will induce jitter on the beam, and a low-noise pickup will be needed to keep the jitter within tolerable limits.

- The high bunch charge, short bunch separation and long bunch trains means that fast-ion effects will occur, with coupled-bunch growth times of around 35 turns, even with a residual gas pressure of 0.1 ntorr. Again, the instability can be suppressed with a bunch-by-bunch feedback system, but there is a concern with the jitter that the feedback system will induce on the beam.

- Measures will be needed to suppress the build-up of electron cloud in the positron damping ring.

- The Touschek lifetime is 155 minutes with the nominal operating conditions. This is long enough for commissioning and tuning purposes.

- Intrabeam scattering will give 20% growth in the horizontal emittance and between 2% and 20% growth in the vertical emittance (depending on the relative contributions of vertical dispersion and betatron coupling to the vertical emittance). A negligible amount of longitudinal emittance growth is expected. The transverse emittance growth is tolerable, but may require that a low-current vertical normalized emittance below 0.02 μm be achieved.

Future studies will compare the beam dynamics in the 3 km lattice presented here, with the 17 km [1] and 6 km [2] lattices proposed elsewhere.

References

[1] TESLA Technical Design Report, DESY 2001-011 (March 2001).

[2] S. Mishra et al, "Studies Pertaining to a Small Damping Ring for the International Linear Collider," FNAL Report (October 2004).

[3] T.O. Raubenheimer, "The Generation and Acceleration of Low-Emittance Flat Beams for Future Linear Colliders", SLAC-Report-387 (1991).

[4] C. Steier, D. Robin, L. Nadolski, W. Decking, Y. Wu, J. Laskar, "Measuring and Optimizing the Momentum Aperture in a Particle Accelerator", Phys. Rev. E 65, 056506 (2002).

[5] D. Robin, C. Steier, J. Laskar, L. Nadolski, "Global Dynamics of the Advanced Light Source Revealed through Experimental Frequency Map Analysis", Phys. Rev. Lett. 85, 558 (2000).

[6] C. Steier et al, "Lattice Model Calibration and Frequency Map Measurements at the ALS", Proceedings of EPAC 2000, Vienna, Austria.

[7] M. Venturini, "Longitudinal Single-Bunch Instabilities in the NLC Main Damping Ring", LBNL-55103 (May 2004).

[8] F. Zimmermann, "Single-Pass Ion Effects in Storage Rings and Linacs", in "Handbook of Accelerator Physics and Engineering" (Edited by A.W. Chao and M. Tigner) pp. 130-131, World Scientific (1999).

[9] K. Ohmi and F. Zimmermann, "Study of Head-Tail Effect Caused by Electron Cloud", Proceedings of EPAC 2000, Vienna, Austria.

[10] H. Wiedemann, "Particle Accelerator Physics II" pp. 328-329, Springer (1995).

[11] K. Bane, "A Simplified Model of Intrabeam Scattering", SLAC-PUB-9226 (June 2002).

[12] J.D. Bjorken and S.K. Mtingwa, "Intrabeam Scattering", Particle Accelerator **13**, 115 (1983).